Treacle's ability to form liquid phase condensates is essential for nucleolar fibrillar center assembly, efficient rRNA transcription and processing, and rRNA gene repair.

Artem K. Velichko[1,2,3], Anastasia P. Kovina[1], Artem V. Luzhin[1,2], Nadezhda V. Petrova[1], Dmitry A. Deriglazov[1], Eugene P. Kazakov[4], Igor I. Kireev[4], Sergey V. Razin[1,5], and Omar L. Kantidze[1,*,§]

[1]Department of Cellular Genomics, Institute of Gene Biology RAS, Moscow, Russia

[2]Center for Precision Genome Editing and Genetic Technologies for Biomedicine, Institute of Gene Biology RAS, Moscow, Russia

[3]Institute for Translational Medicine and Biotechnology, Sechenov First Moscow State Medical University, Moscow, Russia

[4]A.N. Belozersky Institute of Physico-Chemical Biology, Lomonosov Moscow State University, Moscow, Russia

[5]Biological Faculty, Lomonosov Moscow State University, Moscow, Russia

We investigated the role of the nucleolar protein Treacle in organizing and regulating the nucleolus in human cells. Our results support Treacle's capacity to form liquid-phase condensates through electrostatic interactions among molecules. The formation of these biomolecular condensates is crucial for segregating nucleolar fibrillar centers from the dense fibrillar component, as well as ensuring high levels of rRNA gene transcription and accurate pre-rRNA processing. The presence of both the central and C-terminal domains of Treacle is necessary for the creation of liquid-phase condensates. Initiation of phase separation is attributed to the C-terminal domain, while the central domain, characterized by repeated stretches of alternatively charged amino-acid residues, is vital for maintaining the condensate's liquid state. When mutant forms of Treacle, incapable of forming liquid-phase condensates, are overexpressed in cells, it compromises the establishment of fibrillar centers, leading to the suppression of rRNA transcription and disruption of its processing. Additionally, these mutant forms fail to recruit TOPBP1, resulting in the suppression of the DNA damage response in the nucleolus.

[*]Corresponding author: Omar Kantidze (kantidze@gmail.com)

[§]Current address: Quantori LLC, Cambridge, MA, USA

Short title: Phase separation of Treacle promotes rDNA transcription and repair

Introduction

Applying polymer chemistry principles to biological molecules has significantly widened our understanding of membraneless compartments' functioning (Mehta & Zhang, 2022; Mittag & Pappu, 2022). Multiple weak, cooperative, and dynamic interactions underlie the assembly of these self-organized structures, termed biomolecular condensates. Mechanistically, liquid–liquid phase separation (LLPS)—a process of de-mixing that yields a condensed protein-enriched phase and a dilute phase—can mediate the self-assembly of biomolecular condensates. In biological systems, phase separation is mainly a characteristic of multivalent or intrinsically disordered proteins (Banani et al, 2017; Shin & Brangwynne, 2017; Uversky, 2019). Biomolecular condensates serve as functional hubs in diverse cellular processes such as transcription (Sabari et al, 2020), microtubule nucleation (Woodruff et al, 2017), and adaptive stress response (Franzmann & Alberti, 2019).

Nucleolus, a large and complex subnuclear compartment, can also be considered a multicomponent and multilayered biomolecular condensate (Lafontaine et al, 2021). The nucleolus is formed around arrays of ribosomal gene repeats (rDNA), which are transcribed by RNA polymerase I (Pol I) to produce pre-ribosomal RNA (Cerqueira & Lemos, 2019). In the nucleolus, RNAs and hundreds of different proteins are segregated into three immiscible liquid phases: the fibrillar center (FC), which is the inner layer that contains the machinery for rDNA transcription by Pol I; the dense fibrillar component (DFC), which is the intermediate layer that is rich in fibrillarin; the granular component (GC), which is the outer layer that is rich in nucleophosmin (NPM1, B23). Although purified fibrillarin and NPM1 can separate into two distinct phases *in vitro* to create the droplet compartments of DFC and GC, respectively, the nature of the FC droplet compartment remains unclear (Feric et al, 2016). By examining the behavior of the FC in living cells, it has been proposed that the FC's organization is a result of phase separation (Falahati et al, 2016; Falahati & Wieschaus, 2017). Furthermore, several studies have shown that the FC components relocate to the periphery of the nucleolus and aggregate to form large structures called nucleolar caps when Pol I transcription is inhibited by actinomycin D (AMD) or genotoxic drugs (Harding et al, 2015; Korsholm et al, 2019; Reynolds et al, 1964). This transformation process exhibits similarities to the fusion of liquid droplets. Treacle is the main molecule present in the FC, and it has both transcription-dependent and -independent functions (Gal et al, 2022). Its role in ribosome biogenesis is well-documented since it assists in the transcription and processing of rRNA (Gonzales et al, 2005; Lin & Yeh, 2009; Valdez et al, 2004). In addition, it is a master regulator of DNA damage response (DDR) in the nucleolus, mediating recruitment of repair factors to rDNA damage caused by IPpoI-induced breaks, replication stress, or R-loop formation (Ciccia et al, 2014; Korsholm et al, 2019; Larsen et al, 2014; Mooser et al, 2020; Velichko et al, 2021; Velichko et al, 2019). Thus, it acts as a nucleolar hub with both transcriptional and DNA repair functions. The reason for its multifunctionality can be attributed to its possible ability to undergo phase separation and engage in multivalent interactions. Protein structure predictors indicate that Treacle is one of the most

intrinsically disordered proteins. In addition, Treacle's partners in transcription and DNA repair (Pol I and TOPBP1, respectively) also utilize phase separation as a functioning mechanism (Frattini et al, 2021; Ide et al, 2020). Transcription of ribosomal genes can be regulated by phase separation of Pol I, while TOPBP1 condensation can activate the ATR signaling pathway (Frattini et al, 2021; Ide et al, 2020).

In this study, we present experimental evidence that Treacle can form biomolecular condensates, and we thoroughly characterize the structural determinants of Treacle regulating this process. Due to its ability for LLPS, Treacle facilitates the formation of nucleolar FCs, recruiting and concentrating transcription factors at rDNA, and separating FC components from the DFC. Collectively, this segregates rRNA synthesis and its subsequent processing in distinct compartments of the nucleolus. Disruption of Treacle's LLPS capability, leading to the mixing of FC and DFC components, results in reduced efficiency of both processes, equivalent to the consequences of complete depletion of endogenous Treacle. Additionally, we demonstrate that Treacle's phase separation is critical for its interaction with TOPBP1 and activation of DDR in rDNA during genotoxic stress. Our findings reveal the role of Treacle not only as a structural scaffold for FCs but also as a nucleolar hub integrating functions of ribosomal gene transcription, rRNA processing, and preserving rDNA integrity.

Treacle is a scaffold protein for nucleolar FCs and DFCs

First, we defined the role of Treacle in the structural organization of the nucleolus. We employed the CRISPR-Cas9 system to knock out the TCOF1 gene encoding Treacle in HeLa cells to obtain a population of cells lacking Treacle signals (Treacle-negative cells) (Fig. S1A). Immunocytochemical staining of UBF and RPA194 (FC markers), fibrillarin (DFC marker), and B23 and nucleolin (GC markers) revealed that Treacle-positive cells exhibited a classical tripartite nucleolar structure, with Treacle co-localizing with UBF1 and RPA194 (large sub-unit of Pol I) in FCs, fibrillarin in DFCs, and B23 and nucleolin surrounding FCs and DFCs (Fig. 1A). Treacle depletion led to the disappearance of distinct FC and DFC structures, causing RPA194, UBF, and fibrillarin to diffuse throughout the nucleolus and partially relocate to the nucleoplasm (Fig. 1B, S1A), whereas GC components remained unaffected (Fig. 1B). These results indicated that Treacle played a critical role in generating the integrated structure of FCs and DFCs.

Next, we investigated the impact of nucleolar FC disintegration on the efficiency of ribosomal gene transcription and the recruitment of Pol I transcription machinery to rDNA. Chromatin immunoprecipitation revealed reduced occupancy of UBF and RPA194 at the ribosomal gene coding region in Treacle-negative cells, indicating that Treacle amplifies the recruitment rather than initiates the primary binding of transcription machinery to rDNA (Fig. 1C). Depleting Treacle led to substantial suppression of ribosomal gene transcription, though not a complete shutdown, in contrast to the repression induced by AMD (Fig. 1D,E). Furthermore, cells with Treacle depletion also exhibit impairment in the processing of

the 5′ external transcribed spacer, particularly in the cleavage of the A′ site (Fig. 1F) which is one of the initial steps in the 18S rRNA maturation.

In summary, Treacle functions as a scaffold protein in nucleolar FCs, and its depletion compromises both rRNA gene transcription and the processing of rRNA.

Treacle drives the formation of biomolecular condensates

Currently, it has become evident that various scaffold proteins can self-organize through the formation of liquid-phase condensates (Banani et al, 2017; Shin & Brangwynne, 2017). According to protein structure predictors (e.g., AlphaFold, IUPred2, PONDR, FuzDrop), Treacle is one of the most intrinsically disordered proteins (Fig. S2A). To investigate Treacle's ability to self-organize into biomolecular condensates, we initially examined its LLPS properties in an in vitro system.

Purified recombinant Treacle underwent phase separation from the buffer and formed liquid droplets at low salt concentrations and in the presence of dextran as a crowding agent (Fig. 2A). Under these conditions, Treacle efficiently self-organized into large droplets, and their size positively correlated with the strength of crowding (Fig. 2A). These droplets exhibited a spherical shape and frequently fused with one another (Fig. 2B).

To investigate Treacle's ability to self-organize into biomolecular condensates within cells, we generated fusion proteins by linking Treacle to FusionRed (a non-self-dimerizing fluorescent protein) and Arabidopsis thaliana cryptochrome 2 (Cry2), known to oligomerize upon exposure to blue light, facilitating the formation of "optoDroplets" (Shin & Brangwynne, 2017). Expression of this opto–Treacle chimeric protein in HeLa cells revealed foci formation in nucleoli in the absence of blue light, consistent with Treacle's natural tendency to occupy FCs (Fig. 2C; controls in Fig. S2B). Upon blue light exposure, opto–Treacle formed multiple small foci throughout the nucleoplasm (Fig. 2C). We next explored Treacle's ability to form biomolecular condensates when overexpressed as a fusion with the fluorescent protein Katushka2S (referred to as 2S) (Shcherbo et al, 2007). Initially, at low expression levels (16-24 hours post-transfection), Treacle’s fusion protein formed foci only in nucleoli reflecting its natural occupation of FCs (Fig. 2D top panel). However, with increased expression levels (48-72 hours post-transfection), it began to form large spherical structures in the nucleoplasm (Fig.2D). Both intranucleolar and extranucleolar Treacle–2S foci, induced by low and high levels of fusion protein expression respectively, exhibited a spherical shape with an aspect ratio close to one, suggesting susceptibility to surface tension (Fig. 2D). Transmission electron microscopy confirmed the internal homogeneity of Treacle droplets, showing circular structures with homogeneous protein content without any electron-dense or -light regions inside the droplets (Fig. S2C).

Similar to the in vitro-formed Treacle condensates, intracellular Treacle condensates demonstrated the ability to fuse. Our observations reveal that during AMD-induced (Fig. 2E, Movie S1) or DNA damage-

induced (Fig. S2D, Movie S2) rDNA transcriptional repression, nucleolar caps form due to the fusion of intranucleolar Treacle–2S foci. Prolonged live-cell imaging further demonstrated that extranucleolar biomolecular condensates from highly overexpressed Treacle–2S also frequently fuse, indicating dynamic clustering (Fig. 2F, Movie S3).

Liquid condensates exhibit a high molecular exchange rate, often assessed through fluorescence recovery after photobleaching (FRAP) (Ganser & Myong, 2020). FRAP analysis of the entire FC showed slow fluorescence recovery of Treacle, likely due to limited molecule diffusion between different FCs (Fig. S2E). However, when bleaching a specific region within the FC, rapid fluorescence recovery was observed, indicating liquid-like dynamics (Fig. 2G, I). We then analyzed the molecular exchange rate of Treacle in nucleolar caps induced by AMD (Fig. 2H, I) and in extranucleolar droplets induced by high-level expression of Treacle-2S (Fig. 2J, L). Both types of condensates exhibited dynamics consistent with liquid behavior, with slightly higher rates than in FCs. Fluorescence recovery in FCs, nucleolar caps, and extranucleolar condensates never reached the initial values over the analyzed time periods. This suggests that the high molecular exchange rate occurs through the mixing of Treacle molecules within the condensate boundaries and does not involve external diffusion. It is important to note that liquid dynamics were characteristic of Treacle droplets formed 16-48 hours post-transfection, while FRAP analysis of protein dynamics in large extranucleolar droplets 72-96 hours after transfection revealed a shift towards gel-like behavior of the observed condensates (Fig. 2 K,L). Presumably, Treacle condensates undergo a liquid-to-gel phase transition over time or upon reaching a critical protein concentration within the condensate. Thus, using diverse model systems, we illustrated that Treacle can indeed create biomolecular condensates exhibiting the primary features of structures mediated by LLPS.

Treacle's phase separation is regulated by its central and C-terminal domains

We next searched the structural determinants of Treacle contributing to its LLPS characteristics. Despite being a low-complexity protein, Treacle consists of three functional domains: the N-terminal domain (ND) containing the LisH motif, the C-terminal domain (CD) which includes nuclear (NLS) and nucleolar (NOLC) localization signals, and the central or Repeated Domain (RD) consisting of 14 low complexity regions, 11 of which are homologous to each other (Fig. 3A). To identify the domains contributing to LLPS, we generated Treacle mutants with deleted ND (Δ1-83), RD (Δ83-1121), or CD (Δ1121-1488), and overexpressed them in HeLa cells. We decided to overexpress the deletion mutants in wild-type cells and assess their LLPS capacity using several intracellular condensate models: (i) formation of FCs and (ii) nucleolar caps under low expression levels (24 hours post-transfection), and (iii) formation of large extranucleolar condensates under high expression levels (48 hours post-transfection).

The Δ1-83 mutant demonstrated LLPS properties indistinguishable from full-length Treacle: it concentrated in FCs, formed stable nucleolar caps during transcriptional repression, and, upon increased

expression levels, generated numerous large extranucleolar condensates (Fig. 3B, D). Similar to full-length Treacle, Δ1-83 exhibited a high rate of molecular exchange in all types of model condensates (Fig. 3C, E, S3A-C).

The mutant lacking the central domain (Δ83-1121) exhibited LLPS properties distinct from full-length Treacle. Under low expression levels, it failed to concentrate in FCs (Fig. 3F) and diffusely localized in the nucleoplasm (Fig. 3F) while still maintaining a high molecular dynamics rate (Fig. 3G, S3D). During rDNA transcriptional repression, Δ83-1121 did not form classical nucleolar caps but partially redistributed between the nucleolar periphery and nucleoplasm, where it began to form condensates (Fig. 3F). Surprisingly, such relocation was associated with a change in its phase state. FRAP analysis demonstrated that both perinucleolar and nucleoplasmic condensates of Δ83-1121, formed due to nucleolar transcriptional repression, began to transition into a solid state (liquid-solid phase separation,LSPS) (Fig. 3G, S3E-F). It is possible, that without the central domain, Treacle can maintain LLPS only through heterotypic interactions with rRNA. A similar liquid-solid transition was observed for Δ83-1121 under high expression levels. In this case, it no longer formed distinct extranucleolar condensates but merged into a unified pan-nuclear solid-state network (Fig. 3F, G, S3G).

The Δ1121-1488 mutant could not translocate into the nucleus due to the absence of its own NLS (data not shown), so it was additionally fused with the NLS from the SV40 virus. Interestingly, in this form, Δ1121-1488 began to localize in the nucleus but failed to form condensates even under high expression levels (Fig. 3H).

These results suggest that it is the RD that provides the liquid behavior of the Treacle. However, RD is not capable of autonomous condensation and utilizes the CD as a platform for its own nucleation. In turn, CD cannot phase separate independently and requires either RD or rRNA, without which it undergoes a LSPS. Next, we investigated the features of the amino acid sequences of RD and CD that could contribute to these properties.

We started by analyzing the type of low-complexity region (LCR) interactions in full-length Treacle condensates. We first examined the assembly of Treacle droplets *in vitro* in the presence of 1,6-hexanediol, high salt concentrations, or at different pH values. The efficiency of Treacle droplet formation in vitro remained unchanged in the presence of 1,6-hexanediol (Fig. 3I), whereas increasing salt concentration blocked droplet formation (Fig. 3I). Additionally, in vitro, condensation of Treacle was sensitive to changes in pH. The droplet size significantly decreased under acidic conditions (pH 5.5) or alkalization of the environment (pH 10), and was maximal at pH 8.5, corresponding to the isoelectric point for Treacle (Fig. S3H). Intracellular Treacle condensates were also sensitive to changes in ionic strength. Treatment with the cell-permeable salt ammonium acetate disrupted both FCs and extranucleolar condensates formed at low and high Treacle expression levels, respectively (Fig. 3J). In contrast, treatment with 1,6-hexanediol did

not have a similar effect (Fig. 3J). Thus, it is evident that Treacle's LLPS is driven by electrostatic, but not hydrophobic, interactions

Analysis of the charge distribution along the amino acid sequence of Treacle revealed that the repeats in the central domain constitute strong diblock ampholytes, where a block of positive charge is followed by a block of negative charge (Fig. 3K). To determine the physiological importance of this charge distribution, a variant of Treacle, Treacle CS, was created with the same overall net charge but with scrambled blocks (Fig. 3K). In Treacle CS, regions of opposite charge were removed while maintaining the same overall isoelectric point, amino acid composition, and positions of all other residues. As anticipated, scrambling the charges in RD completely blocked Treacle's phase separation ability. Similar to Δ83-1121, CS was unable to form FCs or nucleolar caps (Fig. 3L), remained in a liquid state only in the presence of rRNA (Fig. 3M), and underwent a liquid-solid phase transition during nucleolar transcriptional repression or high levels of overexpression (Fig. 3L, M, S3I-K). This indicates the importance of the charge distribution pattern in RD for maintaining the phase separation properties of Treacle.

The C-terminal domain of Treacle exhibited a significantly positive charge, attributed to the K-rich region at the C-terminus, which is also a NOLC. To analyze the significance of this charge, a Treacle variant with a deletion of the 1350-1488 region (ΔNOLC), including most lysines in CD, was created. As expected, this form of Treacle did not localize to the nucleolus but, nonetheless, was capable of forming individual perinucleolar condensates (Fig. 3N). These condensates demonstrated a liquid state, and the molecular exchange rate within them was even slightly higher than in condensates of full-length Treacle (Fig. 3O, S3L-N). Interestingly, with an increase in the expression level of ΔNOLC, a significant increase in the volume of such condensates was observed, but not an increase in their number (Fig. 3N). This suggests that positively charged lysines in CD serve as nucleation points for autonomous Treacle condensate formation.

In summary, the results indicate that the central and C-terminal domains cooperatively control the phase separation properties of Treacle, while the N-terminal domain does not make a substantial contribution. The highly positively charged CD serves as the nucleation center for RD but exhibits ambivalent phase properties, transitioning from LLPS to LSPS in the absence of rRNA. In turn, RD, with alternating charge blocks in the repeating domains, maintains Treacle condensates in a stably liquid state, thus counteracting rRNA-dependent phase fluctuations in CD. The combination of CD and RD supports a balance of viscoelastic properties in Treacle condensates.

Treacle LLPS is essential for the transcription and processing of rRNA

In the previous part of the study, we demonstrated that Treacle supports the transcription and processing of rRNA. We hypothesized that this functionality of Treacle could be attributed to its ability for LLPS. To test this hypothesis, we significantly downregulated the endogenous Treacle expression using RNA interference (Fig. S4A) and then analyzed the structure of FC/DFC and rRNA transcription levels in the context of the

expression of full-length or LLPS-defective (Δ83-1121 or CS) forms of Treacle. It was observed that compared to the full-length Treacle, which formed classical FC/DFC, each of the LLPS-defective mutants induced dispersion and mixing of FC and DFC components (Fig.4 A,C), similar to what occurs during CRISPR/Cas9-mediated depletion of endogenous Treacle (Fig. 4B,D). In this process, GC did not undergo visible changes (Fig. S4B-D). Additionally, we found that the expression of LLPS-defective mutants significantly reduced the transcription level of rRNA compared to full-length Treacle (Fig.4E). This effect could not be explained by a possible loss of the ability of LLPS-defective mutants of Treacle to bind to rDNA, as both LLPS-defective mutants occupied the coding region of ribosomal repeats in a manner similar to full-length Treacle (Fig. 4F).

Thus, this observation suggests that the LLPS properties of Treacle provide its ability to concentrate components of the transcriptional machinery in FC and separate them from DFC. Moreover, such separation is likely required to maintain highly efficient transcription of ribosomal genes. We hypothesized that the same principle could regulate the role of Treacle in the processing of rRNA. To test this assumption, we depleted the level of endogenous Treacle using RNA interference (Fig. S4A) and then analyzed the spatial localization of newly synthesized 47S-rRNA and its processing level in cells expressing miRNA-resistant full-length or LLPS-defective (Δ83-1121 or CS) forms of Treacle. Microscopy analyses with FISH-labeled rRNA revealed that newly synthesized 47S-rRNA transcript clustered at the periphery of FCs in full-length Treacle-expressing cells, reflecting the radial flow of rRNA from FC to GC (Fig. 4G). However, in cells expressing LLPS-defective Treacle mutants, no clear clustering of newly synthesized rRNA was observed. Instead, the newly synthesized transcripts were diffusely mixed with Δ83-1121 and CS Treacle (Fig. 4G). In cells with depleted endogenous Treacle, nascent pre-rRNA transcripts were similarly mixed with delocalized UBF (Fig. 4H). Finally, reverse transcription-qPCR analysis confirmed that cells overexpressing LLPS-defective Treacle mutants demonstrated impairment of 5′ external transcribed spacer processing compared to cells overexpressing full-length Treacle (Fig.4I). Thus, it can be concluded that the mixing of FC and DFC components induced by the expression of LLPS-defective Treacle, as well as the depletion of endogenous Treacle, disrupts the directional traffic of nascent pre-rRNA from FC to DFC and further to GC, which may be a cause of inefficient processing.

Our results indicate that Treacle's phase separation properties provide separation of FC and DFC, leading to the spatial segregation of rRNA synthesis and its subsequent processing. The mixing of FC and DFC components due to the disruption of Treacle's LLPS ability results in reduced efficiency of both processes, equivalent in consequences to the complete depletion of endogenous Treacle.

Treacle phase separation is essential for DDR activation in ribosomal genes under genotoxic stress conditions

Previous studies have demonstrated that Treacle is critically required for the induction of DDR in ribosomal genes under certain types of stress (Korsholm et al, 2019; Larsen et al, 2014; Mooser et al, 2020; Velichko et al, 2021; Velichko et al, 2019). Here, we aimed to investigate the contribution of Treacle's phase separation to rDNA damage response. To induce rDNA damage, we used the widely used chemotherapeutic drug etoposide (VP16), which acts as a topoisomerase II poison inducing double-strand breaks (DSBs) (Bax et al, 2019). Treatment of cells with 90 μM VP16 for 30 minutes resulted in the rapid recruitment of TOPBP1 to nucleoli and its colocalization with Treacle (Fig. 5A). Furthermore, proximity ligation assay (PLA) analysis conducted after DNA damage induction provided evidence of a physical association between TOPBP1 and Treacle (Fig. 5B). The reduction of endogenous Treacle levels, achieved either through RNA interference (Treacle kd) or CRISPR/Cas9-mediated depletion (Treacle kn), effectively blocked the relocalization of TOPBP1 to nucleoli and its occupancy of rDNA (Fig. 5C, S5A). Interestingly, with RNA interference, a substantial amount of Treacle still remained in nucleoli (Fig. S5A). However, this amount was insufficient to facilitate its interaction with TOPBP1, likely due to the need for specific stoichiometric ratios for efficient interaction.

Next, we investigated whether the interaction between Treacle and TOPBP1 in Treacle kd cells could be restored by the overexpression of different Treacle variants. The results of immunocytochemical analysis and chromatin immunoprecipitation with antibodies against TOPBP1 indicated that the expression of full-length Treacle in Treacle kd cells effectively restored the VP16-induced interaction between Treacle and TOPBP1, as well as the enrichment of TOPBP1 at the promoters of ribosomal genes. However, the expression of LLPS-defective forms of Treacle (Δ83-1121 or CS) did not lead to such restoration (Fig. 5D,E).

The response to DNA damage involves the activation of various signaling kinases and the recruitment of different repair factors to the DNA break site. Using chromatin immunoprecipitation followed by quantitative PCR (ChIP-qPCR) with antibodies against a panel of DNA repair proteins, it was confirmed that VP16 indeed induced DDR at the promoters of rDNA, including the activation of ATM/ATR kinases, phosphorylation of histone H2AX, and recruitment of repair factors such as 53BP1 and BRCA1 (Fig. 5F, S5C). As expected, nucleolar DDR was fully controlled by the interaction between Treacle and TOPBP1, as the knockdown of either of these proteins led to a dramatic reduction in VP16-induced repair signaling at rDNA (Fig. 5F, S5B,C). Finally, it was confirmed that nucleolar DDR could be efficiently restored in Treacle kd cells by overexpressing full-length Treacle, but not its LLPS-defect mutants (Δ83-1121 or CS) (Fig. 5G, S5D). Thus, we can conclude that the phase separation by Treacle plays a crucial role in facilitating its binding to TOPBP1 and activating DDR in conditions of genotoxic damage to rDNA.

Discussion

The nucleolus is a multicomponent phase condensate formed on the platform of rRNA, which is processed and incorporated into assembling ribosomes simultaneously with migration from FCs to DFCs and further to GC. Each of the nucleolar compartments provides a special environment formed by the demixing of a particular protein that constitutes a permanent component of a given compartment. Essential client proteins are subsequently recruited to this phase condensate. The constitutive components of DFC and GC are nucleolin and nucleophosmin (B23), respectively (Feric et al, 2016; Lafontaine et al, 2021). The debate continues regarding which protein plays a comparable role in FCs. The results of our study suggest that the phosphoprotein Treacle serves as the scaffold protein for nucleolar fibrillar centers in human cells. This aligns entirely with the findings of the E. Calo group, demonstrating that the evolutionary emergence of Treacle correlates with the appearance of the three-partite nucleolus in amniotes (Jaberi-Lashkari et al, 2023). They demonstrated that the introduction of human Treacle into zebrafish, which lack a competent ortholog for FC formation, induced the reorganization of the nucleolar structure from bipartite to tripartite, accompanied by the formation of FC-like structures.

Here, we demonstrated that Treacle organizes nucleolar FCs through its LLPS properties and also investigated the underlying mechanism leading to the phase separation of Treacle. The phase behavior of polymers is determined by interactions through associative motifs, referred to as stickers, separated by spacers, which are not the primary driving forces for phase separation (Choi et al, 2020). In Treacle, stickers consist of K/R and E/D residues in repeated disordered regions (RD) which generate alternating charged blocks. Meanwhile, a large number of glycine, proline, and glutamine residues, well-known as disorder-promoting residues (Romero et al, 2001; Theillet et al, 2013), can serve as effective spacers.

While the central domain of Treacle is responsible for its liquid behavior, this domain alone is unable to undergo autonomous phase separation within the cell. To undergo phase separation, the central domain requires a positively charged C-terminal domain, acting as a platform for nucleation. The mechanism by which the C-terminal domain facilitates nucleation is not entirely clear. We hypothesize that positively charged K residues in the C-terminal domain may interact with negatively charged E/D residues in RD, utilizing electrostatic interactions. Interestingly, the zebrafish ortholog of Treacle is homologous to human Treacle only in the central domain, lacking a homologous sequence for the C-terminal domain. This likely accounts for its inability to condense and form fully functional FC.

Endogenous Treacle may undergo post-translational modifications. Specifically, the central domain of Treacle is known to be heavily phosphorylated and ubiquitinated (Mooser et al, 2020; Werner et al, 2018; Werner et al, 2015). Currently, the role of these modifications is primarily attributed to facilitating interactions with partner proteins such as CUL3KBTBD8 or NOLC1 (Werner et al, 2018). However, it is known that phosphorylation can modulate phase separation, particularly by enhancing or reducing the polyampholytic properties of disordered regions (Yamazaki et al, 2022). As LLPS of Treacle relies on its

polyampholytic nature, we do not exclude that post-translational ubiquitination and phosphorylation may alter charge ratios in its central domain, thereby modulating ampholytic properties and finely tuning phase separation.

The synthesis of 47S pre-rRNA occurs at the FC/DFC boundary, while primary processing initiates in the DFC. DFC formation is mediated by phase separation of fibrillarin gathered on pre-rRNA scaffold and is maintained as long as there is a directed radial flow of rRNA from FC to DFC (Yao et al, 2019). The role of Treacle in ensuring rRNA processing has been repeatedly described in the literature (Calo et al, 2018; Gonzales et al, 2005), but the mechanism of this phenomenon remained unclear. We demonstrated that the efficiency of rRNA processing is compromised not only with the complete depletion of endogenous Treacle but also with the expression of LLPS-defective mutants of Treacle. This led us to propose that Treacle facilitates rRNA processing not only through the direct recruitment of specific factors but also by organizing the cooperative structure of FC/DFC and separating FC components from DFC. Disruption and mixing of FC and DFC components due to Treacle's impaired LLPS properties may interfere with the radial flow of rRNA, thus hindering its normal processing.

Additionally, we explored the role of Treacle’s phase separation in nucleolar DDR. Treacle's well-known partner, TOPBP1, plays a crucial role in the activation of ATR during DNA replication stress (Day et al, 2021). The interaction between TOPBP1 and Treacle is essential for nucleoli-specific DDR and replication stress response (Mooser et al, 2020; Velichko et al, 2021; Velichko et al, 2019). This interaction occurs via phosphoserines 1227/1228 in a conserved acidic motif of C-terminal domain of Treacle (Mooser et al, 2020). However, we showed that Treacle with intact phosphoserines 1227/1228 but unable to undergo LLPS loses the ability to interact with TOPBP1 during genotoxic stress. This implies that for interaction with TOPBP1 and subsequent activation of nucleolar DDR, Treacle must also possess corresponding phase separation characteristics.

In conclusion, our study unveils Treacle's role not merely as a structural scaffold for FC/DFC but as a nucleolar hub protein that integrates functions in ribosomal gene transcription, rRNA processing, and rDNA repair.

Materials and methods

Cell culture and drug treatment

Human HeLa (ATCC® CCL-2™) were cultured in DMEM (PanEco) supplemented with 10% fetal bovine serum (FBS; HyClone/GE Healthcare) and penicillin/streptomycin. The cells were cultured at 37°C in a conventional humidified CO_2 incubator. DNA damage was induced by the treatment of cells with 90 µM etoposide (Sigma-Aldrich, #E1383) for 30 min or 1 h. For rRNA transcription inhibition, cells were treated with 0,05 µg/ml actinomycin D (Sigma-Aldrich, #A1410) or 20 µM CX-5461 for 3 h. To obtain 1,6-hexanediol (HD)-treated cells, HeLa cells were incubated with 5% 1,6-HD (Sigma-Aldrich, #240117) in serum-free medium at 37°C in a humidified atmosphere for 10 min. To obtain ammonium acetate-treated cells, HeLa cells were incubated with 200 mM ammonium acetate in a complete culture medium at room temperature for 5 min.

Plasmid constructs

For the FusionRED-Treacle-Cry2 (opto-Treacle) construct, the full-length Treacle was amplified by PCR from cDNA with primer set #1 (Supplementary Table 1) using KAPA High-Fidelity DNA Polymerase (KAPA Biosystems, KE2502). The forward and reverse primers contained XhoI sites. The amplified fragment was inserted into the FusionRed-C vector (Evrogen, FP411) linearized with XhoI. The Cry2 fragment was amplified by PCR from the plasmid pHR-mCh-Cry2WT (Addgene, #101221) with primer set #2 (Supplementary Table 1) digested with NheI and inserted into pFusionRed-Treacle linearized with NheI using NheI enzyme.

For the FusionRED-FUS-Cry2 construct, the FUS was amplified by PCR from the plasmid pHR-FUSN-mCh-Cry2WT (Addgene, #101223) with primer set #3 (Supplementary Table 1) using KAPA High-Fidelity DNA Polymerase (KAPA Biosystems, KE2502). The forward and reverse primers contained BspEI and KpnII sites respectively. The amplified fragment was inserted into the pFusionRed-C vector (Evrogen, FP411). The Cry2 fragment was amplified by PCR from the plasmid pHR-mCh-Cry2WT (Addgene, #101221) with primer set #2 (Supplementary Table 1) digested with NheI and inserted into pFusionRed-Treacle using NheI enzyme.

To generate Treacle-GFP or Treacle-Katushka2S constructs, the full-length Treacle was amplified by PCR from cDNA with primer set #4 (Supplementary Table 1) using KAPA High-Fidelity DNA Polymerase (KAPA Biosystems, KE2502). The forward and reverse primers contained BglII and BamHI sites respectively. The amplified fragment was inserted into the pTurboGFP-C (Evrogen, FP511) or pKatushka2S-C (Evrogen, FP761) vectors using BglII/BamHI restriction/ligation.

Treacle Δ1-83 deletion mutant was constructed based on the pTreacle-GFP full or pTreacle-2S full plasmid using iProof High-Fidelity DNA polymerase with primer set #5 (Supplementary Table 1). The resulting DNA template after PCR was reprecipitated and treated with the DpnI restriction enzyme. In the next step, the desired DNA template was purified on an agarose gel, phosphorylated with T4 Polynucleotide Kinase (T4 PNK), and ligated.

To obtain the charge-scrambled Treacle-GFP or Treacle-2S (Treacle-GFP CS or Treacle-2S CS), a fragment encoding 137-1130 aa of Treacle was removed from the pTreacle-GFP or pTreacle-2S plasmid using EcoR1 and HindIII restrictases. This fragment was then replaced with a synthetic sequence encoding the amino acid sequence with the necessary changes (see Supplementary Table 2).

Treacle Δ83-1121 deletion mutant was constructed based on the pTreacle-GFP full or pTreacle-2S full plasmid using iProof High-Fidelity DNA polymerase with primer set #6 (Supplementary Table 1). The resulting DNA template after PCR was reprecipitated and treated with the DpnI restriction enzyme. In the next step, the desired DNA template was purified on an agarose gel, phosphorylated with T4 Polynucleotide Kinase (T4 PNK), and ligated.

Treacle Δ1121-1488-NLS mutant was constructed based on the pTreacle-GFP full or pTreacle-2S full plasmid using iProof High-Fidelity DNA polymerase with primer set #7 (Supplementary Table 1). The resulting DNA template after PCR was reprecipitated and treated with the DpnI restriction enzyme. In the next step, the desired DNA template was purified on an agarose gel, phosphorylated with T4 Polynucleotide Kinase (T4 PNK), and ligated.

For the generation of Treacle ΔNOLC (Δ1350-1488) mutant, fragments were amplified by PCR from the pTreacle-GFP plasmid with primer set #8 (Supplementary Table 1). The forward and reverse primers contained BglII and BamHI sites respectively. The amplified fragment was inserted into either the pTurboGFP-C (Evrogen, FP511) or pKatushka2S-C (Evrogen, FP761) vectors using BglII/BamHI restriction/ligation.

Gene knockdown

RNA interference experiments were performed using Lipofectamine 3000 transfection reagent (Thermo Scientific) following the manufacturer's instructions. The cells were transfected with 50 nM Treacle/TCOF1 siRNA (the sequences of the siRNA is provided in Supplementary Table S3) or 50 nM TOPBP1 (Santa Cruz Biotechnology, #sc-41068).

For CRISPR/Cas9-mediated knockout, two single guide RNAs (sgRNA) to first exon of the TCOF1 gene were designed using the guide RNA design tool (www.atum.bio/eCommerce/cas9/input). The sgRNA targeting sequences were separately cloned into the px330mCherry (Addgene #98750). A list of all oligonucleotides is provided in Supplementary Table S3. The plasmids were co-transfected into HeLa cells with LTX transfection reagent (Invitrogen). 5-7 days after transfection cells were fixed and immunostained with required antibodies.

Fluorescence microscopy

For immunostaining, cells were grown on microscope slides. All samples were fixed in 1% formaldehyde in PBS for 15 min at room temperature and treated with 1% Triton X-100 for permeabilization. Cells were washed in PBS and then incubated with antibodies in PBS supplemented with 1% BSA and 0.05% Tween 20 for 1 h at room temperature or overnight at 4°C. Then the cells were washed with PBS three times (5 min each time). The primary antibodies bound to antigens were visualized using Alexa Fluor 488-conjugated secondary antibodies. The DNA was counterstained with the fluorescent dye 4,6-diamino-2-phenylindole (DAPI) for 10 min at room temperature. The samples were mounted using Dako fluorescent mounting medium (Life Technologies). The immunostained samples were analyzed using a Zeiss AxioScope A.1 fluorescence microscope (objectives: Zeiss N-Achroplan 40 ×/0.65 and EC Plan-Neofluar 100 ×/1.3 oil; camera: Zeiss AxioCam MRm; acquisition software: Zeiss AxioVision Rel. 4.8.2; Jena, Germany) or STELLARIS 5 Leica confocal microscope (objectives: HC PL APO 63x/1.40 oil CS2). The images were processed using ImageJ software (version 1.44) and analyzed using CellProfiler software (version 3.1.5). 3D reconstruction of *xyz* confocal datasets (*z*-stacks) was performed using Leica LAS-X software. Antibodies used in the study are listed in Supplementary Table 7.

Cell sorting

Cells were transiently transfected with required plasmids using LTX transfection reagent (Invitrogen) or immunostained with required antibodies. Cell sorting was performed using an SH800 Cell Sorter (Sony) with a laser tuned to 488 nm for green fluorescence and 561 nm for red fluorescence. Gates were set with reference to negative controls. A minimum of $2x10^6$ events was collected for ChIP or RNA extraction.

RNA extraction and RT-qPCR

After sorting, living or immunostained cells were pelleted by centrifugation at 3000 g for 5′ at 4°C. The supernatant was discarded. Total RNA was isolated from the pellet as described (Hrvatin et al, 2014). All

RNA samples were further treated with DNase I (Thermo Scientific) to remove the residual DNA. RNA (1 µg) was reverse transcribed in a total volume of 20 µl for 1 h at 42°C using 0.4 µg of random hexamer primers and 200 U of reverse transcriptase (Thermo Scientific) in the presence of 20 U of ribonuclease inhibitor (Thermo Scientific). The cDNA obtained was analyzed by quantitative polymerase chain reaction (qPCR) using the CFX96 real-time PCR detection system (Bio-Rad Laboratories). The PCRs were performed in 20 µl reaction volumes that included 50 mM Tris–HCl (pH 8.6), 50 mM KCl, 1.5 mM $MgCl_2$, 0.1% Tween-20, 0.5 µM of each primer, 0.2 mM of each dNTP, 0.6 µM EvaGreen (Biotium), 0.2 U of Hot Start Taq Polymerase (Sibenzyme) and 50 ng of cDNA. Primers used in the study are listed in Supplementary Table 4.

Chromatin immunoprecipitation (ChIP) and ChIP-seq analysis

Living cells were fixed for 15 min with 1% formaldehyde at room temperature, and crosslinking was quenched by adding 125 mM glycine for 5 min. Cell sorting was performed if needed. Cells were harvested in PBS, and nuclei were prepared by incubation in FL buffer (5 mM PIPES, pH 8.0, 85 mM KCl, 0.5% NP40) supplemented with Protease Inhibitor Cocktail (Bimake) and Phosphatase Inhibitor Cocktail (Bimake) for 30 min on ice. Next, chromatin was sonicated in RIPA buffer (10 mM Tris–HCl, pH 8.0, 140 mM NaCl, 1% Triton X-100, 0.1% sodium deoxycholate, 0.1% SDS) with a VirSonic 100 to an average length of 200-500 bp. Per ChIP reaction, 10–20 µg chromatin was incubated with 2–4 µg antibodies overnight at 4°C. The next day, Protein A/G Magnetic Beads (Thermo Scientific) were added to each sample and incubated for 4 h at 4°C. Immobilized complexes were washed two times for 10 min at 4°C in low salt buffer (20 mM Tris-HCl, pH 8.0, 150 mM NaCl, 2 mM EDTA, 0.1% SDS, 1% Triton X-100) and high salt buffer (20 mM Tris–HCl, pH 8.0, 500 mM NaCl, 2 mM EDTA, 0.1% SDS, 1% Triton X-100). Samples were incubated with RNase A (Thermo Scientific) for 30 min at room temperature. The DNA was eluted from the beads and de-crosslinked by proteinase K digestion for 4 h at 55°C and subsequent incubation at 65°C for 12 h. Next, DNA was purified using phenol/chloroform extraction and analyzed by qPCR. The qPCR primers used for ChIP analysis are listed in Supplementary Table 5.

The sequencing libraries were then prepared with NEBNext Ultra II kit according manufacturer's protocol. Final libraries were PCR amplificated and adapter dimers were cleaned with 1:1 MagPure magnetic beads (Magen Biotechnology). Resulted DNA was resuspended in 30 mkl 10 mM Tris-HCl buffer ph 8.0 and were sequenced on Illumina machine. Chip-seq reads were mapped to the reference human genome hg38 assembly using Bowtie v2.2.3 with the '–very-sensitive' mode. Non-uniquely mapped reads, possible PCR and optical duplicates were filtered out using SAMtools v1.5. The bigWig files with the ratio of RPKM normalized ChIP-seq signal to the input were generated using deepTools v3.4.2 bamCompare function.

Cool files was generated, merged and normalized using cooler version 0.8.11 (https://github.com/open2c/cooler).

Electron microscopy

Twenty-four hours after transfection, cells were fixed with 2.5% neutralized glutaraldehyde in the requisite buffer for 2 h at room temperature, post-fixed with 1% aqueous OsO4, and embedded in Epon. Sections of 100 nm thickness were cut and counterstained with uranyl acetate and lead citrate. Sections were examined and photographed with a JEM 1400 transmission electron microscope (JEOL, Japan) equipped with a QUEMESA bottom-mounted CCD-camera (Olympus SIS, Japan) and operated at 100 kV.

In vitro Treacle condensation

Recombinant human Treacle protein (#YHG52701, Atagenix) was diluted with LLPS buffer (20 mM Tris-HCl, pH 7.4, 1 mM EDTA, 100 mM KCl) to a final concentration of 10 µM protein. Treacle LLPS was examined in the absence and presence of 1-10% dextran as a crowding agent. To test the effects of NaCL or 1,6-hexandiol on Treacle LLPS, NaCL or 1,6-hexandiol was added to the LLPS buffer with 10% PEG at 500 mM or 10% concentrations, respectively. The mixtures were analyzed on the Zeiss AxioScope A.1 fluorescence microscope equipped for brightfield imaging.

Live-cell imaging

Cells were seeded in 35-mm glass-bottom dishes twelve hours before transfection with the plasmid. Twenty-four hours after transfection, Hoechst 33342 (Cell Signaling Technology) was added to the medium at a final concentration of 1 µg/ml, and the cells were incubated for 20 min at 37°C. Hoechst-containing medium was replaced with a complete fresh medium before the cells underwent live-cell imaging using a STELLARIS 5 Leica confocal microscope (objectives: HC PL APO 63x/1.40 oil CS2) equipped with an incubation chamber to provide a humidified atmosphere at 37°C with 5% CO_2. For observation of liquid droplet behavior, z-stack time-lapses were taken. Maximum intensity projections are shown, but all findings were confirmed on a single plane.

Optodroplet assay

Cells were seeded in 35-mm glass-bottom dishes and were transfected with Treacle-FusionRed-Cry2 plasmid using LTX transfection reagent (Invitrogen) 24 h before imaging. Twenty-four hours after transfection, Hoechst 33342 was added to the medium at a final concentration of 1 μg/ml, and the cells were incubated for 10 min at 37°C. Hoechst-containing medium was replaced with a complete fresh medium before the cells underwent live-cell imaging using a STELLARIS 5 Leica confocal microscope (objectives: HC PL APO 63x/1.40 oil CS2) equipped with an incubation chamber to provide a humidified atmosphere at 37°C with 5% CO2. Droplet formation was induced with light pulses at 488 nm (blue light, 1% laser power) for 10 sec, and z-stack images were captured every 60 sec in the absence of blue light.

FRAP analysis

Samples for FRAP were prepared as described above for live-cell imaging experiments. FRAP experiments were performed on STELLARIS 5 Leica confocal microscope (objectives: HC PL APO 63x/1.40 oil CS2) equipped with an incubation chamber to provide a humidified atmosphere at 37°C with 5% CO_2. Regions of interest were bleached using 405-nm laser (1% laser power).

The measurements involved 3 prebleaching frames, one flashes of bleaching (1% of laser power), and 28 postbleaching frames (5 s/frame). Individual FRAP traces were normalized to maximal prebleach and minimal postbleach intensities.

Proximity ligation assay

After drug treatments or at 24 h post-transfection, cells were fixed for 15 min with 1% formaldehyde at room temperature and permeabilized with 1% Triton X-100. Next, cells were subjected to the proximity ligation assay (PLA) using the Duolink Green (Sigma-Aldrich) according to the manufacturer's instructions. Briefly, cells were blocked, incubated with appropriate primary antibodies overnight at 4°C, and then incubated with PLA probes, which are secondary antibodies (anti-mouse-IgG and anti-rabbit-IgG) conjugated to unique oligonucleotides. Samples were then treated with a ligation solution followed by an amplification solution containing polymerase and fluorescently labeled oligonucleotides, allowing rolling-circle amplification and detection of discrete fluorescent dots. Some samples after the PLA protocol were additionally counterstained with Alexa-Fluor-488- or Alexa-Fluor-594-conjugated (Molecular Probes) secondary antibody. The DNA was counterstained with DAPI for 10 min at room temperature. The samples were mounted using Dako fluorescent mounting medium (Life Technologies) and analyzed using STELLARIS 5 Leica confocal microscope (objectives: HC PL APO 63x/1.40 oil CS2). The images were analyzed using ImageJ software (version 1.44).

Transcription labeling

For EU incorporation, the cells were incubated with 100 μM EU (Sigma-Aldrich) for 2 hr at 37°C. Then, the cells were washed three times with PBS and fixed in ice-cold methanol for 10 min. The samples were then processed using a Click-iT EU Imaging Kit (Life Technologies) according to the manufacturer's recommendations.

Single molecule RNA Fluorescentin in situ Hybridization (smFISH)

All single-molecule RNA FISH probes were designed as described (Yao et al, 2019) and labeled with FITS on the 3'ends (Supplementary Table 6). Cells were fixed with 4% PFA for 15 min, followed by permeabilization with 1% Triton X-100 for 10 min. Cells were incubated in 10% formamide/2x SSC for 10 min at room temperature and then were hybridizated with 5 nM each of RNA probes in 50% formamide/2x SSC at 37◦C for 16 hours. After hybridization, the cells were washed 10% formamide/2x SSC for 30 min at 37◦C.

Acknowledgments

This work was supported by RSF grant 21-74-10018. Confocal microscopy studies were supported by grant 075-15-2019-1661 from the Ministry of Science and Higher Education of the Russian Federation.

Author contributions: O.L.K., A.K.V., and S.V.R. conceived the study. A.K.V. and O.L.K. designed the experiments. A.K.V., A.P.K., A.V.L., and D.A.D. performed most of the experiments. E.P.K. and I.I.K. performed transmission electron microscopy imaging. O.L.K. and A.K.V. wrote the manuscript with assistance from the other authors.

Competing interests: The authors declare no competing interests.

Data and materials availability: All data needed to evaluate the conclusions in the paper are present in the paper and/or the Supplementary Materials.

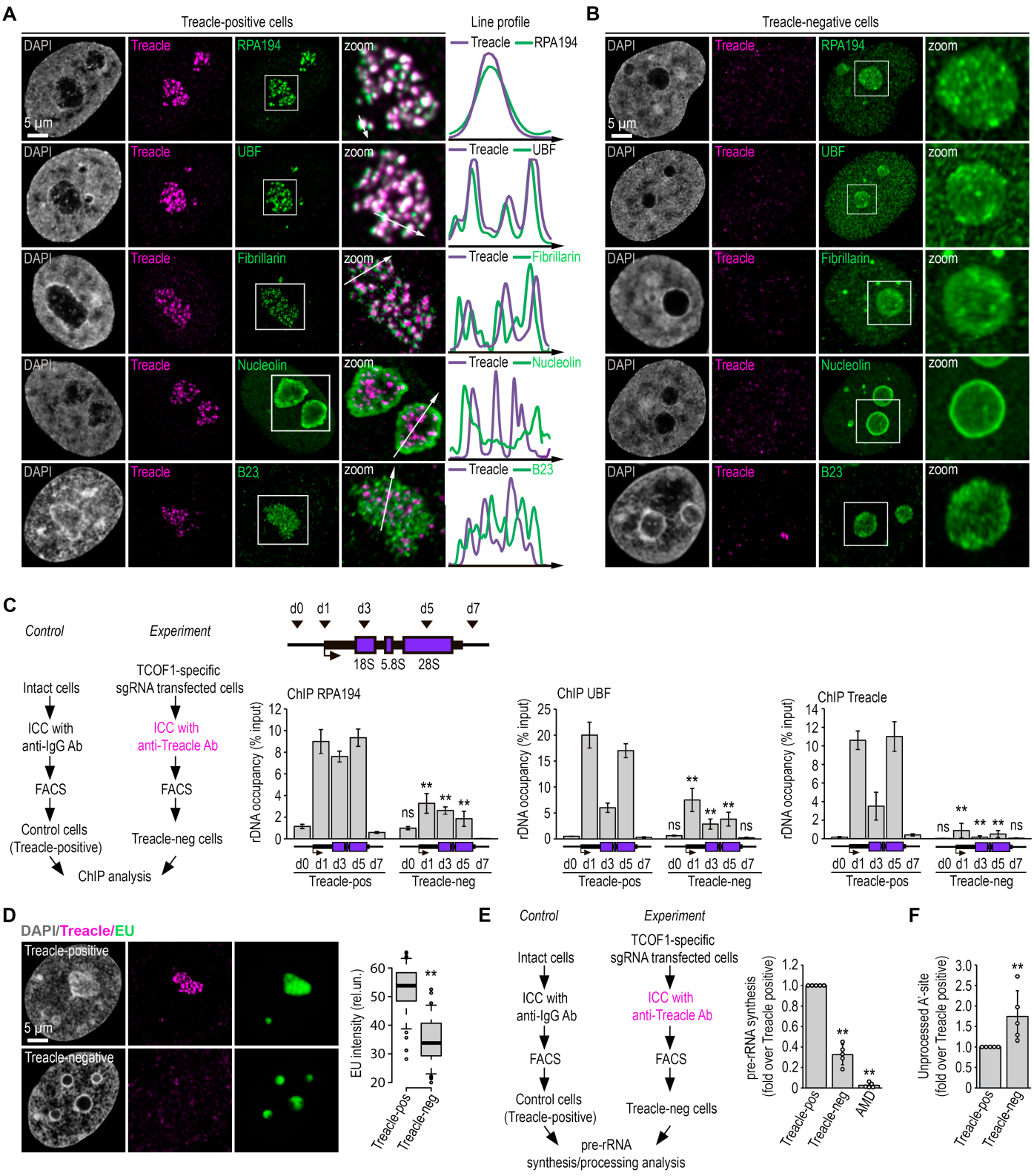
A
Treacle-positive cells
Line profile
DAPI
Treacle
RPA194
UBF
Fibrillarin
Nucleolin
B23
zoom
5 µm
B
Treacle-negative cells
C
Control
Experiment
Intact cells
ICC with anti-IgG Ab
FACS
Control cells (Treacle-positive)
TCOF1-specific sgRNA transfected cells
ICC with anti-Treacle Ab
Treacle-neg cells
ChIP analysis
d0 d1 d3 d5 d7
18S 5.8S 28S
ChIP RPA194
ChIP UBF
ChIP Treacle
rDNA occupancy (% input)
Treacle-pos
Treacle-neg
ns
D
DAPI/Treacle/EU
Treacle-positive
Treacle-negative
EU intensity (rel.un.)
E
pre-rRNA synthesis/processing analysis
pre-rRNA synthesis (fold over Treacle positive)
AMD
F
Unprocessed A'-site (fold over Treacle positive)

Fig. 1 Treacle is a scaffold protein for nucleolar FCs and DFCs.

(A) Intact HeLa cells (Treacle-positive) were fixed and co-immunostained with Treacle and with either RPA194, UBF, Fibrillarin, B23 or Nucleolin antibodies. DNA was stained with DAPI (gray). Cells were analyzed by laser scanning confocal microscopy. Representative images of cells and nucleoli (magnified images) are shown. Co-localization analysis was performed on the merged images. Graphs illustrate quantification in arbitrary units of fluorescence distribution along the lines shown in the figures. **(B)** HeLa cells were transfected with a construct coding CRISPR/Cas9 and sgRNA to the TCOF1 gene. After 7-10 days after transfection, the cells were fixed and immunostained with Treacle and either RPA194, UBF, Fibrillarin, B23 or Nucleolin antibodies. Cells were analyzed by laser scanning confocal microscopy. Representative images of Treacle-negative cells and nucleoli (magnified images) are shown. **(C)** HeLa cells were transfected with a construct coding CRISPR/Cas9 and sgRNA to the TCOF1 gene (experiment). After 7-10 days after transfection cell were fixed, immunostained with Treacle antibodies and subjected to cell sorting to obtain Treacle-negative populations. The sorted cell fractions were used for ChIP analysis with either Treacle, RPA194 or UBF antibodies. Intact HeLa cells were fixed, immunostained with IgG antibodies, passed through all FACS-related procedure and used as a control (Treacle-positive). ChIP was followed by qPCR using the d0, d1, d3, d5, d7 primers to the rRNA gene (positioned as indicated on the scheme). Data are represented relative to the input. Values are means ±SD from at least three independent replicates. **(D)** HeLa cells were transfected with a construct coding CRISPR/Cas9 and sgRNA to the TCOF1 gene. After 7-10 days after transfection the cells were pulsed with EU (100 μM for 2 hr), fixed and immunostained with Treacle antibodies. EU (green) was revealed by click chemistry. The DNA was stained with DAPI (gray). Representative images of Treacle-positive and Treacle-negative HeLa cells are shown. Quantification of EU fluorescence intensities in Treacle-positive and Treacle-negative HeLa cells are show in the right panel (n>500). **(E)** HeLa cells were transfected with a construct coding CRISPR/Cas9 and sgRNA to the TCOF1 gene. After 7-10 days after transfection the cells were fixed, immunostained with Treacle antibodies and subjected to cell sorting into Treacle-negative populations. The sorted cell fractions were used for RNA extraction. Intact HeLa cells were fixed, stained with IgG antibodies, passed through all FACS-related procedure and used as a control (Treacle-positive). RT-qPCR was performed; it shows levels of 47S pre-rRNA normalized to GAPDH mRNA. Normalized pre-rRNA level in Treacle-positive cells is set to 1. Values are mean ± SD. The calculation is presented for 5 biological replicates. **(F)** Hela cells were processed as described in (E). It shows levels of A'-site contained unprocessed rRNA normalized to GAPDH mRNA. Normalized unprocessed rRNA level in Treacle-positive cells is set to 1. Values are mean ± SD. The calculation is presented for 5 biological replicates.

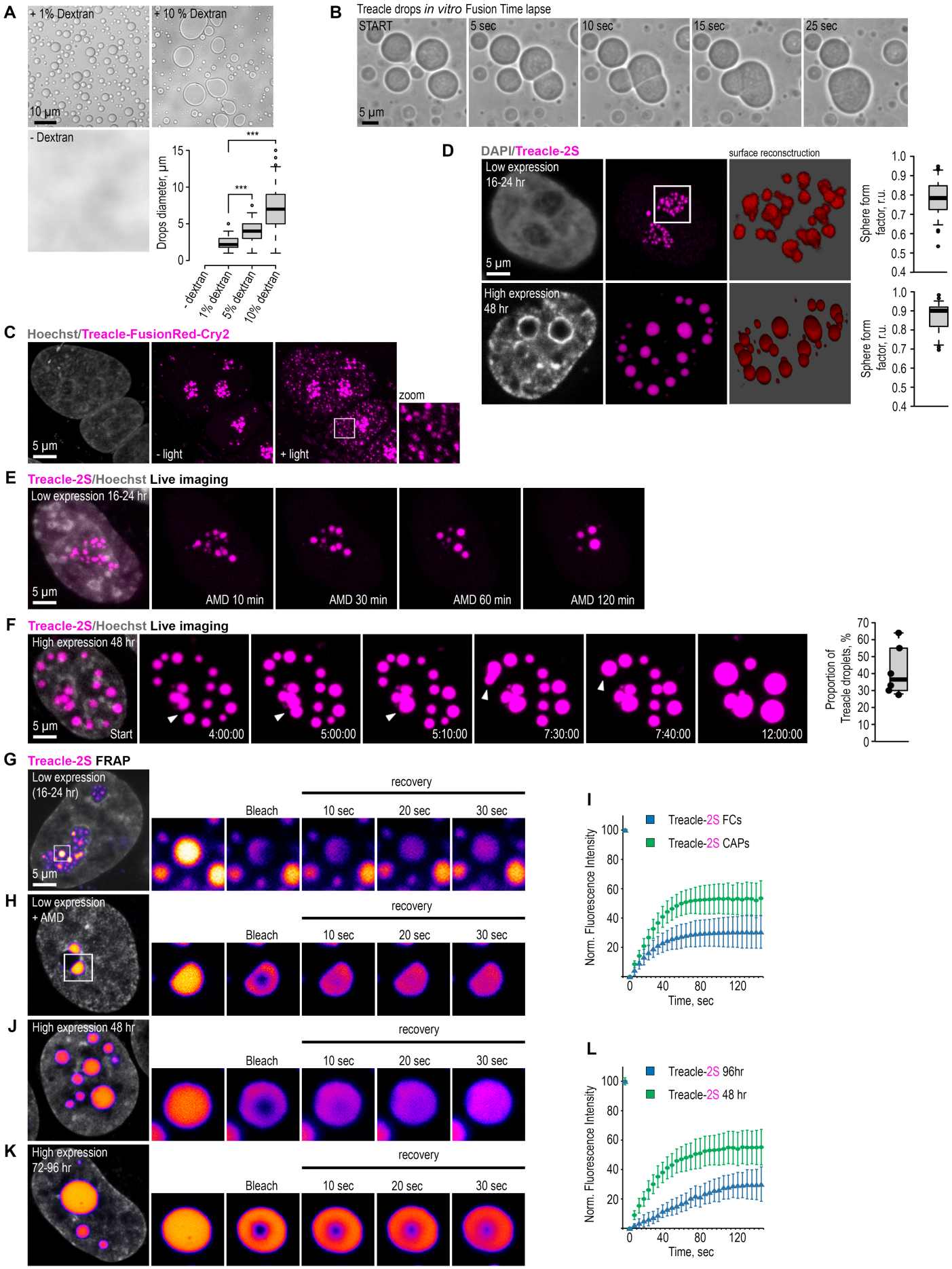
A
+ 1% Dextran
+ 10 % Dextran
10 µm
- Dextran
Drops diameter, µm
***
***
- dextran
1% dextran
5% dextran
10% dextran
B
Treacle drops in vitro Fusion Time lapse
START
5 sec
10 sec
15 sec
25 sec
5 µm
C
Hoechst/Treacle-FusionRed-Cry2
5 µm
- light
+ light
zoom
D
DAPI/Treacle-2S
surface reconsctruction
Low expression
16-24 hr
5 µm
High expression
48 hr
Sphere form factor, r.u.
E
Treacle-2S/Hoechst Live imaging
Low expression 16-24 hr
5 µm
AMD 10 min
AMD 30 min
AMD 60 min
AMD 120 min
F
Treacle-2S/Hoechst Live imaging
High expression 48 hr
5 µm
Start
4:00:00
5:00:00
5:10:00
7:30:00
7:40:00
12:00:00
Proportion of Treacle droplets, %
G
Treacle-2S FRAP
Low expression
(16-24 hr)
5 µm
recovery
Bleach
10 sec
20 sec
30 sec
H
Low expression
+ AMD
J
High expression 48 hr
K
High expression
72-96 hr
I
Treacle-2S FCs
Treacle-2S CAPs
Norm. Fluorescence Intensity
Time, sec
L
Treacle-2S 96hr
Treacle-2S 48 hr

Fig. 2. Treacle drives the formation of nuclear condensates.

(A) Purified recombinant Treacle underwent phase separation from the buffer and formed liquid droplets in the presence of 1-10% dextran as a crowding agent. The size of Treacle drops was measured (n>500). **(B)** Drops of recombinant Treacle were time-lapse imaged. Representative images of drop fusion events are shown. **(C)** HeLa cells were transfected with Treacle-FusionRed-Cry2 (opto-Treacle) construct. Formation of opto-Treacle drops was induced with blue light illumination of the cells for 10 sec. DNA was stained with Hoechst 33342 (gray). Representative images are shown. **(D)** HeLa cells were transfected with Treacle-Katushka2S (Treacle-2S) at a quantity of 50 ng plasmids per $2x10^5$ cells. For low or high levels of expression analysis, the cells were fixed 16-24 or 48 h after transfection, respectively. DNA was stained with DAPI (gray). Cells were analyzed by laser scanning confocal microscopy. Surface reconstructions of Treacle-2S drops are shown in the right panel. Graphs illustrate quantification in arbitrary units of the 3D analysis of Treacle-2S drops' shape by LasX software. Sphere form factor = sphere area/particle area. **(E)** 16-24 h after transfection with Treacle-2S, HeLa cells were treated with 0.05µg/ml actinomycin D (AMD) to induce rDNA transcriptional repression and time-lapse imaged for 120 minutes. **(F)** 48 h after transfection with Treacle-2S, HeLa cells were live time-lapse imaged. Representative images of cells with Treacle-2S drops fusion events are shown. Graphs illustrate the frequency of fusion Treacle condensates per cell for 12 hours. The calculation is presented for 6 biological replicates of 10 cells each. **(G)** HeLa cells were transiently transfected with Treacle-2S. 16-24 h after transfection FRAP analysis of Treacle-labelled fibrillar center (FCs) dynamics was performed. Part of one FC was bleached, and fluorescence recovery was monitored. Representative time-lapse images of the photobleached FC are shown (magnified images). **(H)** 16-24 h after transfection with Treacle-2S, HeLa cells were treated with 0.05µg/ml AMD to induce the formation of nucleolar caps. Part of the nucleolar cap was bleached, and fluorescence recovery was monitored. Representative time-lapse images of photobleached nucleolar caps are shown (magnified images). **(I)** Graphs illustrate the quantification of the Treacle-2S FRAP analysis described in (G) and (H). Each trace represents an average of measurements for at least twenty FCs or nucleolar caps; error bars represent SD. **(J)** HeLa cells were transiently transfected with Treacle-2S. 48 h after transfection, FRAP analysis of Treacle-2S extranucleolar condensates dynamics was performed. Part of one drop was bleached, and fluorescence recovery was monitored. Representative time-lapse images of photobleached Treacle-2S extranucleolar condensate are shown (magnified images). **(K)** HeLa cells were transiently transfected with Treacle-2S. 72-96 h after transfection, HeLa cells were processed as described in (J). **(L)** Graphs illustrate the quantification of the Treacle-2S FRAP analysis described in (J) and (K). Each trace represents an average of measurements for at least twenty Treacle-2S condensates; error bars represent SD.

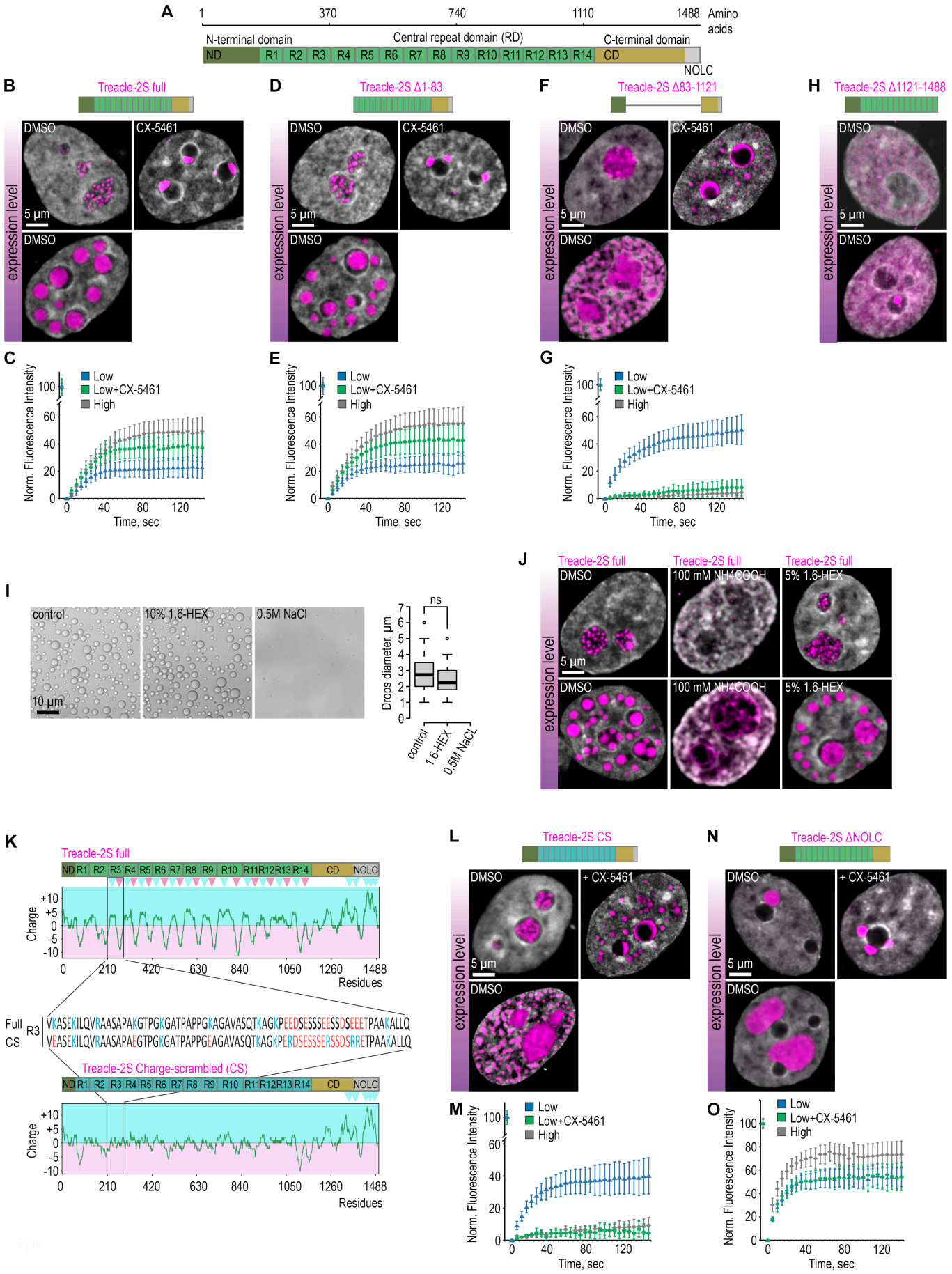
A
1
370
740
1110
1488
Amino acids
N-terminal domain
Central repeat domain (RD)
C-terminal domain
ND R1 R2 R3 R4 R5 R6 R7 R8 R9 R10 R11 R12 R13 R14 CD
NOLC
B
Treacle-2S full
D
Treacle-2S Δ1-83
F
Treacle-2S Δ83-1121
H
Treacle-2S Δ1121-1488
DMSO
CX-5461
expression level
5 µm
C
E
G
Low
Low+CX-5461
High
Norm. Fluorescence Intensity
Time, sec
I
control
10% 1.6-HEX
0.5M NaCl
10 µm
Drops diameter, µm
ns
control
1.6-HEX
0,5M NaCL
J
Treacle-2S full
100 mM NH4COOH
5% 1.6-HEX
K
Treacle-2S full
Charge
Residues
Full
CS
R3
VKASEKILQVRAASAPAKGTPGKGATPAPPGKAGAVASQTKAGKPEEDSESSSEESSDSEEETPAAKALLQ
VEASEKILQVRAASAPAEGTPGKGATPAPPGEAGAVASQTKAGKPERDSESSSERSSDSRRETPAAKALLQ
Treacle-2S Charge-scrambled (CS)
L
Treacle-2S CS
+ CX-5461
M
N
Treacle-2S ΔNOLC
O

Fig. 3. Treacle's phase separation is regulated by its central and C-terminal domains

(A) The structure of the most common isoform of Treacle. Treacle isoform d (1488 amino acids, 152 kDa, NP_001128715.1) is encoded by the Treacle transcript variant 4. It is an intrinsically disordered protein with N-terminal (ND, 1–83 aa), C-terminal (CD, 1121–1488 aa) regions, and central repeated domain (RD, 83–1121 aa) consisting of 14 low complexity regions (LCR). **(B)** HeLa cells were transfected with 2S-fused full-length Treacle. For low or high levels expression analysis cells were cultivated 16-24 or 48 h after transfection respectively. The expression level is indicated by the colored zone to the left of the cell images. HeLa cells with low expression level were additionally treated with CX-5461 to induce rDNA transcriptional repression DNA and subsequent nucleolar cap formation. Cells were fixed and analyzed by laser scanning confocal microscopy. DNA was stained with DAPI (gray). Representative images of full-length Treacle-2S condensate are shown. **(C)** HeLa cells were transiently transfected 2S-fused full-length Treacle and cultivated as described in (B). FRAP analysis of 2S-fused full-length Treacle condensates dynamics was performed. Graphs illustrate quantification of FRAP analysis for each type of Treacle-formed condensates (FCs, nucleolar caps, extranucleolar condensates). Each trace represents an average of measurements for at least twenty for each type of condensates; error bars represent SD. **(D)** HeLa cells were transfected with 2S-fused Treacle Δ1-83 deletion mutant and processed as described in (B). **(E)** HeLa cells were transfected with 2S-fused Treacle Δ1-83 deletion mutant and cultivated as described in (B). FRAP analysis of 2S-fused Treacle Δ1-83 condensates dynamics was performed as described in (C). **(F)** HeLa cells were transfected with 2S-fused Treacle Δ83-1121 deletion mutant and processed as described in (B). **(G)** HeLa cells were transfected with 2S-fused Treacle Δ83-1121 deletion mutant and cultivated as described in (B). FRAP analysis of 2S-fused Treacle Δ83-1121 condensates dynamics was performed as described in (C). **(H)** HeLa cells were transfected with Treacle Δ1121-1488 deletion mutant fused with 2S and nuclear localization signal (NLS) from simian virus 40 (SV40). For low or high levels expression analysis cells were cultivated 16-24 or 48 h after transfection respectively. The expression level is indicated by the colored zone to the left of the cell images. Cells were fixed and analyzed by laser scanning confocal microscopy. DNA was stained with DAPI (gray). Representative images of cells are shown. **(I)** Purified recombinant Treacle underwent phase separation in the presence of 10% 1,6-hexandiol (1,6-HEX) or 500 mM sodium chloride. In each case, 10% dextran was used as a crowding agent. The size of Treacle drops was measured (n>500). **(J)** HeLa cells were transfected with 2S-fused full-length Treacle. For low or high levels expression analysis, cells were cultivated 16-24 or 48 h after transfection respectively. The expression level is indicated by the colored zone to the left of the cell images. Cells were treated with 5% 1,6-hexandiol (1,6-HEX) for 10 min or 200 mM ammonium acetate for 5 min. Cells were fixed and analyzed by laser scanning confocal microscopy. DNA was stained with DAPI (gray). Representative images of cells are shown. **(K)** Charge plots of full-length Treacle (top panel) and charge-scrambled Treacle (Treacle CS) form (bottom panel) are shown. Positive and negative charge blocks are depicted by blue and red triangles, respectively. Charge distribution was calculated as the sum of the charges (Arg and Lys, +1; Glu and Asp, −1;) in the 25 amino acids window range. The center of the panel shows the aligned amino acid sequences of the third LCR of RD for the full Treacle and Treacle CS. **(L)** HeLa cells were transfected with charge-scrambled 2S-fused Treacle (Treacle-2S CS) and processed as described in (B). **(M)** HeLa cells were transfected with Treacle-2S CS and cultivated as described in (B). FRAP analysis of Treacle-2S CS condensates dynamics was performed as described in (C). **(N)** HeLa cells were transfected with 2S-fused Treacle Δ1350-1488 deletion mutant (Treacle-2S ΔNOLC) and processed as described in (B). **(O)** HeLa cells were transfected with Treacle-2S ΔNOLC and cultivated as described in (B). FRAP analysis of Treacle-2S ΔNOLC condensates dynamics was performed as described in (C).

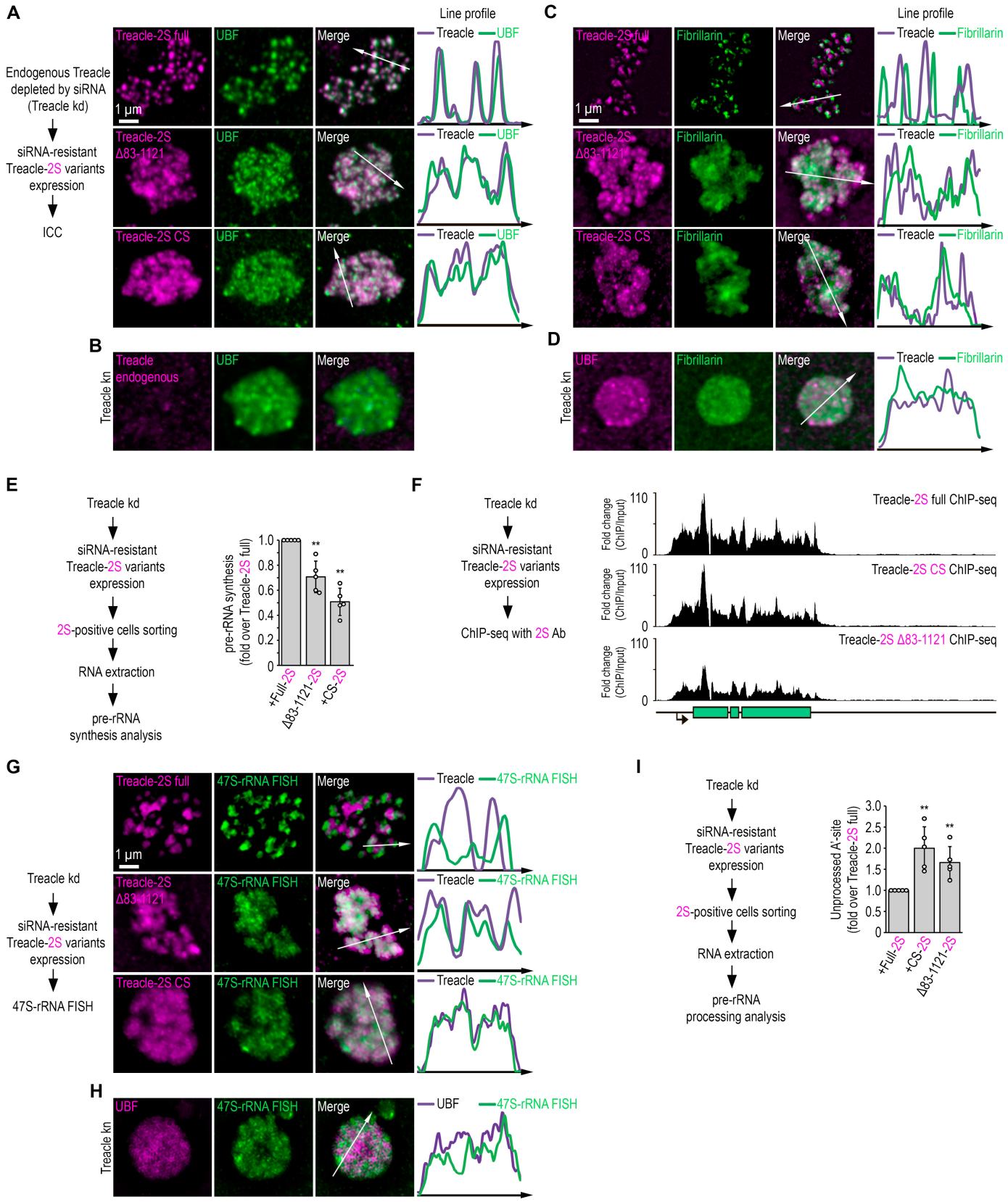
A
Endogenous Treacle depleted by siRNA (Treacle kd)
siRNA-resistant Treacle-2S variants expression
ICC
Treacle-2S full
UBF
Merge
Line profile
Treacle
UBF
1 µm
Treacle-2S Δ83-1121
Treacle-2S CS
B
Treacle kn
Treacle endogenous
C
Fibrillarin
D
E
Treacle kd
siRNA-resistant Treacle-2S variants expression
2S-positive cells sorting
RNA extraction
pre-rRNA synthesis analysis
pre-rRNA synthesis (fold over Treacle-2S full)
+Full-2S
Δ83-1121-2S
+CS-2S
F
ChIP-seq with 2S Ab
Fold change (ChIP/Input)
Treacle-2S full ChIP-seq
Treacle-2S CS ChIP-seq
Treacle-2S Δ83-1121 ChIP-seq
G
47S-rRNA FISH
H
I
Unprocessed A'-site (fold over Treacle-2S full)

Fig. 4. Treacle LLPS is essential for the transcription and processing of rRNA

(A) Endogenous Treacle was depleted by siRNA-mediated knockdown (Treacle kd). Next, Treacle-depleted cells were transfected with siRNA-resistant 2S-fused full-length Treacle (Treacle-2S full), charge-scrambled Treacle (Treacle-2S CS) or Treacle Δ83-1121 deletion mutant (Treacle-2S Δ83-1121). Cells were fixed 16-24 after transfection and immunostained with anti-UBF antibodies. Cells were analyzed by laser scanning confocal microscopy. Representative images of magnified nucleoli are shown. Co-localization analysis was performed on the merged images. Graphs illustrate quantification in arbitrary units of Treacle-2S variants and UBF fluorescence distribution along the lines shown in the figures. **(B)** HeLa cells were transfected with a construct coding CRISPR/Cas9 and sgRNA to the TCOF1 gene. After 7-10 days after transfection, the cells were fixed and immunostained with Treacle and UBF antibodies. Cells were analyzed by laser scanning confocal microscopy. Representative images of Treacle-negative nucleolus (magnified images) are shown. **(C)** HeLa cells were processed as described in (A) and immunostained with Fibrillarin antibodies. **(D)** HeLa cells were processed as described in (B) and immunostained with Fibrillarin and UBF antibodies. Cells were analyzed by laser scanning confocal microscopy. Representative images of Treacle-negative nucleolus (magnified images) are shown. **(E)** HeLa cells were processed as described in (A). Cells were fixed 16-24 after transfection and subjected to cell sorting into 2S-positive populations. The sorted cell fractions were used for RNA extraction. RT-qPCR was performed; it shows levels of 47S pre-rRNA normalized to GAPDH mRNA. Normalized pre-rRNA level in 2S-fused full-length Treacle-positive cells is set to 1. Values are mean ± SD. The calculation is presented for 5 biological replicates. **(F)** HeLa cells were processed as described in (A). Cells were fixed 16-24 after transfection and subjected to ChIP-seq analysis with Katushka2S antibodies. ChIP-seq signal were normalized to the input. **(G)** HeLa cells were processed as described in (A). Cells were fixed 16-24 after transfection and stained for rRNA (revealed by single-molecule FISH, smFISH). Cells were analyzed by laser scanning confocal microscopy. Representative images of magnified nucleoli are shown. Co-localization analysis was performed on the merged images. Graphs illustrate quantification in arbitrary units of Treacle-2S variants and smFISH fluorescence distribution along the lines shown in the figures. **(H)** HeLa cells were processed as described in (B) and stained with UBF antibodies and smFISH. Representative images of Treacle-negative nucleolus (magnified images) are shown. **(I)** HeLa cells were processed as described in (A). Cells were fixed 16-24 after transfection and subjected to cell sorting into 2S-positive populations. The sorted cell fractions were used for RNA extraction. RT-qPCR was performed; it shows levels of A'-site contained unprocessed rRNA normalized to GAPDH mRNA. Normalized unprocessed rRNA level in 2S-fused full-length Treacle-positive cells is set to 1. Values are mean ± SD. The calculation is presented for 5 biological replicates.

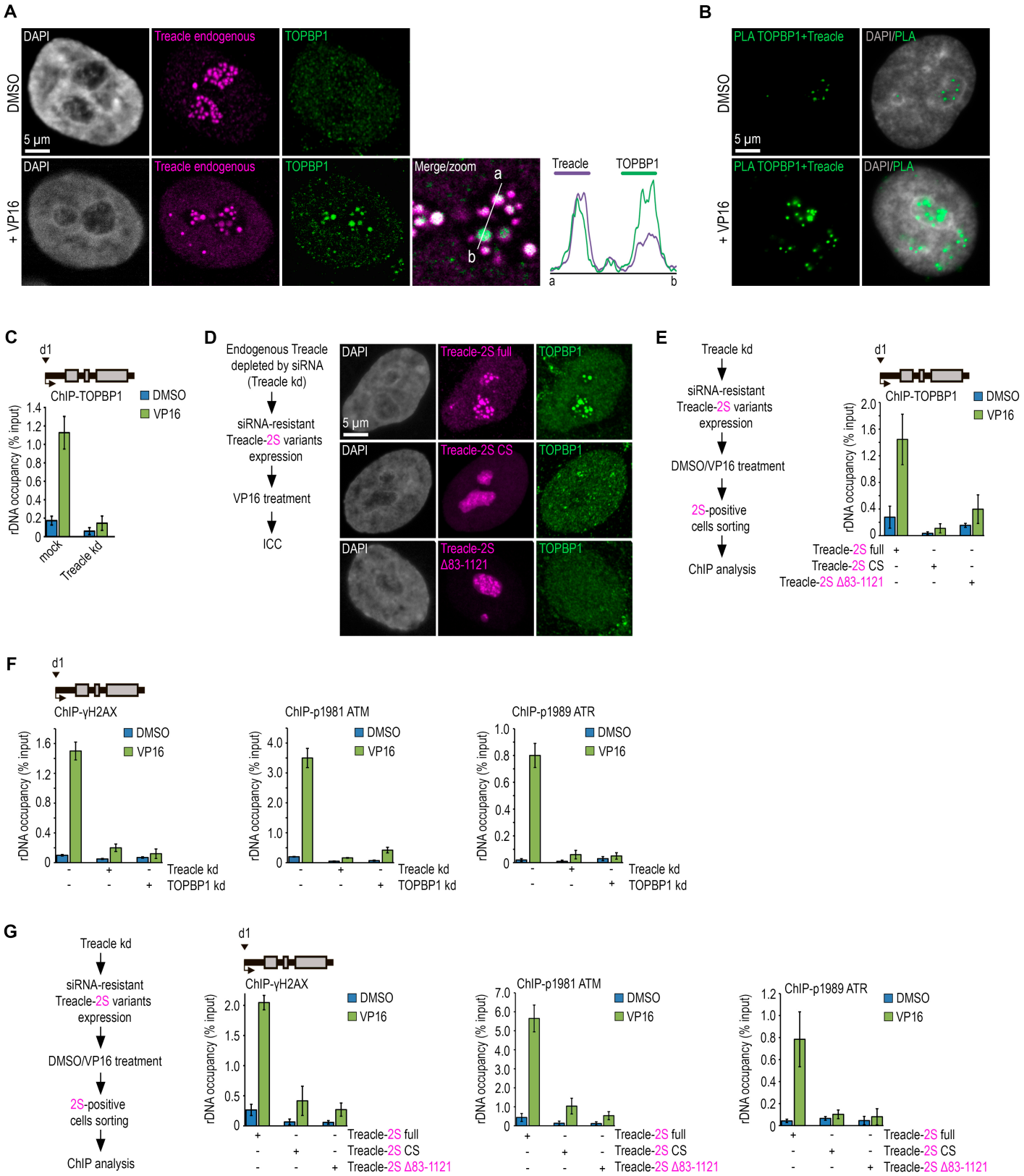
A
DMSO
+ VP16
DAPI
Treacle endogenous
TOPBP1
Merge/zoom
5 µm
a
b
Treacle
TOPBP1
B
PLA TOPBP1+Treacle
DAPI/PLA
C
d1
ChIP-TOPBP1
DMSO
VP16
rDNA occupancy (% input)
mock
Treacle kd
D
Endogenous Treacle depleted by siRNA (Treacle kd)
siRNA-resistant Treacle-2S variants expression
VP16 treatment
ICC
Treacle-2S full
Treacle-2S CS
Treacle-2S Δ83-1121
E
Treacle kd
siRNA-resistant Treacle-2S variants expression
DMSO/VP16 treatment
2S-positive cells sorting
ChIP analysis
F
ChIP-γH2AX
ChIP-p1981 ATM
ChIP-p1989 ATR
Treacle kd
TOPBP1 kd
G

Fig. 5. Treacle phase separation is essential for DDR activation in ribosomal genes under genotoxic stress conditions

(A) Control (DMSO-treated) and VP16-treated (90 μM, 30 min) HeLa cells were stained for Treacle (magenta) and TOPBP1 (green) and analyzed by laser scanning confocal microscopy. The DNA was stained with DAPI (gray). Co-localization analysis was performed on the merged images (magnified images). Graphs illustrate quantification in arbitrary units of Treacle and TOPBP1 fluorescence distribution along the lines shown in the figures. **(B)** Control (DMSO-treated) and VP16-treated (90 μM, 30 min) HeLa cells were subjected to PLA with antibodies against TOPBP1 and Treacle. DNA was stained with DAPI (gray). PLA detection of Treacle-TOPBP1 interactions is visible as distinct green, fluorescent dots. **(C)** Control (mock-treated) HeLa cells or cells with siRNA-mediated Treacle knockdown (Treacle kd) were treated with DMSO or VP16 (90 μM, 30 min). ChIP experiments were performed with antibodies against TOPBP1. ChIP was followed by qPCR using the d1 primers to the promoter of the rRNA gene (positioned as indicated on the scheme). Data are represented relative to the input. Values are means ±SD from at least three independent replicates. **(D)** Endogenous Treacle was depleted by siRNA-mediated knockdown of the TCOF1 gene (Treacle kd). Next, Treacle-depleted cells were transfected with plasmid constructs encoding siRNA-resistant 2S-fused full-length Treacle, 2S-fused Treacle Δ83-1121, or 2S-fused charge-scrambled mutant Treacle (Treacle-2S CS). 24 h after transfection, cells were treated with VP16 (90 μM for 30 min), fixed and stained for TOPBP1 (green) and analyzed by laser scanning confocal microscopy. The DNA was stained with DAPI (gray). **(E)** Endogenous Treacle was depleted by siRNA-mediated knockdown of the TCOF1 gene (Treacle kd). Treacle-depleted cells were transfected with plasmid constructs encoding siRNA-resistant 2S-fused full-length Treacle, 2S-fused Treacle Δ83-1121, or 2S-fused charge-scrambled mutant Treacle (Treacle-2S CS). 24 h after transfection, cells were treated with DMSO or VP16 (90 μM for 30 min) and fixed. Cells were subjected to cell sorting into 2S-positive populations. At least $2x10^6$ sorted cells were used for ChIP with TOPBP1 antibodies. ChIP was followed by qPCR using the d1 primers to the promoter of the rRNA gene (positioned as indicated on the scheme). Data are represented relative to the input. Values are means ±SD from at least three independent replicates. **(F)** Intact HeLa cells and cells siRNA-depleted for either Treacle (Treacle kd) or TOPBP1 (TOPBP1 kd) were treated with DMSO or 90 μM VP16 for 30 min. ChIP experiments were performed with antibodies against phospho-ATR (pATR; Ser1989), phospho-ATM (pATM; Ser1981) or γH2AX antibodies. ChIP was followed as described in (E). **(G)** HeLa cells were processed as described in (E). At least $2x10^6$ sorted cells were used for ChIP with phospho-ATR (pATR; Ser1989), phospho-ATM (pATM; Ser1981) or γH2AX antibodies. ChIP was followed by qPCR using the d1 primers to the promoter of the rRNA gene (positioned as indicated on the scheme). Data are represented relative to the input. Values are means ±SD from at least three independent replicates.

References

Banani SF, Lee HO, Hyman AA, Rosen MK (2017) Biomolecular condensates: organizers of cellular biochemistry. *Nat Rev Mol Cell Biol* **18:** 285-298

Bax BD, Murshudov G, Maxwell A, Germe T (2019) DNA Topoisomerase Inhibitors: Trapping a DNA-Cleaving Machine in Motion. *Journal of molecular biology* **431:** 3427-3449

Calo E, Gu B, Bowen ME, Aryan F, Zalc A, Liang J, Flynn RA, Swigut T, Chang HY, Attardi LD, Wysocka J (2018) Tissue-selective effects of nucleolar stress and rDNA damage in developmental disorders. *Nature* **554:** 112-117

Cerqueira AV, Lemos B (2019) Ribosomal DNA and the Nucleolus as Keystones of Nuclear Architecture, Organization, and Function. *Trends in genetics : TIG* **35:** 710-723

Choi JM, Holehouse AS, Pappu RV (2020) Physical Principles Underlying the Complex Biology of Intracellular Phase Transitions. *Annual review of biophysics* **49:** 107-133

Ciccia A, Huang JW, Izhar L, Sowa ME, Harper JW, Elledge SJ (2014) Treacher Collins syndrome TCOF1 protein cooperates with NBS1 in the DNA damage response. *Proc Natl Acad Sci U S A* **111:** 18631-18636

Day M, Parry-Morris S, Houghton-Gisby J, Oliver AW, Pearl LH (2021) Structural basis for recruitment of the CHK1 DNA damage kinase by the CLASPIN scaffold protein. *Structure (London, England : 1993)* **29:** 531-539 e533

Falahati H, Pelham-Webb B, Blythe S, Wieschaus E (2016) Nucleation by rRNA Dictates the Precision of Nucleolus Assembly. *Curr Biol* **26:** 277-285

Falahati H, Wieschaus E (2017) Independent active and thermodynamic processes govern the nucleolus assembly in vivo. *Proc Natl Acad Sci U S A* **114:** 1335-1340

Feric M, Vaidya N, Harmon TS, Mitrea DM, Zhu L, Richardson TM, Kriwacki RW, Pappu RV, Brangwynne CP (2016) Coexisting Liquid Phases Underlie Nucleolar Subcompartments. *Cell* **165:** 1686-1697

Franzmann TM, Alberti S (2019) Protein Phase Separation as a Stress Survival Strategy. *Cold Spring Harb Perspect Biol* **11**

Frattini C, Promonet A, Alghoul E, Vidal-Eychenie S, Lamarque M, Blanchard MP, Urbach S, Basbous J, Constantinou A (2021) TopBP1 assembles nuclear condensates to switch on ATR signaling. *Mol Cell* **81:** 1231-1245 e1238

Gal Z, Nieto B, Boukoura S, Rasmussen AV, Larsen DH (2022) Treacle Sticks the Nucleolar Responses to DNA Damage Together. *Front Cell Dev Biol* **10:** 892006

Ganser LR, Myong S (2020) Methods to Study Phase-Separated Condensates and the Underlying Molecular Interactions. *Trends Biochem Sci* **45:** 1004-1005

Gonzales B, Henning D, So RB, Dixon J, Dixon MJ, Valdez BC (2005) The Treacher Collins syndrome (TCOF1) gene product is involved in pre-rRNA methylation. *Hum Mol Genet* **14:** 2035-2043

Harding SM, Boiarsky JA, Greenberg RA (2015) ATM Dependent Silencing Links Nucleolar Chromatin Reorganization to DNA Damage Recognition. *Cell Rep* **13:** 251-259

Hrvatin S, Deng F, O'Donnell CW, Gifford DK, Melton DA (2014) MARIS: method for analyzing RNA following intracellular sorting. *PloS one* **9:** e89459

Ide S, Imai R, Ochi H, Maeshima K (2020) Transcriptional suppression of ribosomal DNA with phase separation. *Sci Adv* **6**

Jaberi-Lashkari N, Lee B, Aryan F, Calo E (2023) An evolutionarily nascent architecture underlying the formation and emergence of biomolecular condensates. *Cell Rep* **42:** 112955

Korsholm LM, Gal Z, Lin L, Quevedo O, Ahmad DA, Dulina E, Luo Y, Bartek J, Larsen DH (2019) Double-strand breaks in ribosomal RNA genes activate a distinct signaling and chromatin response to facilitate nucleolar restructuring and repair. *Nucleic acids research* **47:** 8019-8035

Lafontaine DLJ, Riback JA, Bascetin R, Brangwynne CP (2021) The nucleolus as a multiphase liquid condensate. *Nat Rev Mol Cell Biol* **22:** 165-182

Larsen DH, Hari F, Clapperton JA, Gwerder M, Gutsche K, Altmeyer M, Jungmichel S, Toledo LI, Fink D, Rask MB, Grofte M, Lukas C, Nielsen ML, Smerdon SJ, Lukas J, Stucki M (2014) The NBS1-Treacle complex controls ribosomal RNA transcription in response to DNA damage. *Nat Cell Biol* **16:** 792-803

Lin CI, Yeh NH (2009) Treacle recruits RNA polymerase I complex to the nucleolus that is independent of UBF. *Biochem Biophys Res Commun* **386:** 396-401
Mehta S, Zhang J (2022) Liquid-liquid phase separation drives cellular function and dysfunction in cancer. *Nat Rev Cancer* **22:** 239-252
Mittag T, Pappu RV (2022) A conceptual framework for understanding phase separation and addressing open questions and challenges. *Mol Cell* **82:** 2201-2214
Mooser C, Symeonidou IE, Leimbacher PA, Ribeiro A, Shorrocks AK, Jungmichel S, Larsen SC, Knechtle K, Jasrotia A, Zurbriggen D, Jeanrenaud A, Leikauf C, Fink D, Nielsen ML, Blackford AN, Stucki M (2020) Treacle controls the nucleolar response to rDNA breaks via TOPBP1 recruitment and ATR activation. *Nat Commun* **11:** 123
Reynolds RC, Montgomery PO, Hughes B (1964) Nucleolar "Caps" Produced by Actinomycin D. *Cancer Res* **24:** 1269-1277
Romero P, Obradovic Z, Li X, Garner EC, Brown CJ, Dunker AK (2001) Sequence complexity of disordered protein. *Proteins* **42:** 38-48
Sabari BR, Dall'Agnese A, Young RA (2020) Biomolecular Condensates in the Nucleus. *Trends Biochem Sci* **45:** 961-977
Shcherbo D, Merzlyak EM, Chepurnykh TV, Fradkov AF, Ermakova GV, Solovieva EA, Lukyanov KA, Bogdanova EA, Zaraisky AG, Lukyanov S, Chudakov DM (2007) Bright far-red fluorescent protein for whole-body imaging. *Nat Methods* **4:** 741-746
Shin Y, Brangwynne CP (2017) Liquid phase condensation in cell physiology and disease. *Science (New York, NY)* **357**
Theillet FX, Kalmar L, Tompa P, Han KH, Selenko P, Dunker AK, Daughdrill GW, Uversky VN (2013) The alphabet of intrinsic disorder: I. Act like a Pro: On the abundance and roles of proline residues in intrinsically disordered proteins. *Intrinsically disordered proteins* **1:** e24360
Uversky VN (2019) Protein intrinsic disorder and structure-function continuum. *Progress in molecular biology and translational science* **166:** 1-17
Valdez BC, Henning D, So RB, Dixon J, Dixon MJ (2004) The Treacher Collins syndrome (TCOF1) gene product is involved in ribosomal DNA gene transcription by interacting with upstream binding factor. *Proc Natl Acad Sci U S A* **101:** 10709-10714
Velichko AK, Ovsyannikova N, Petrova NV, Luzhin AV, Vorobjeva M, Gavrikov AS, Mishin AS, Kireev, II, Razin SV, Kantidze OL (2021) Treacle and TOPBP1 control replication stress response in the nucleolus. *J Cell Biol* **220**
Velichko AK, Petrova NV, Luzhin AV, Strelkova OS, Ovsyannikova N, Kireev, II, Petrova NV, Razin SV, Kantidze OL (2019) Hypoosmotic stress induces R loop formation in nucleoli and ATR/ATM-dependent silencing of nucleolar transcription. *Nucleic acids research* **47:** 6811-6825
Werner A, Baur R, Teerikorpi N, Kaya DU, Rape M (2018) Multisite dependency of an E3 ligase controls monoubiquitylation-dependent cell fate decisions. *eLife* **7**
Werner A, Iwasaki S, McGourty CA, Medina-Ruiz S, Teerikorpi N, Fedrigo I, Ingolia NT, Rape M (2015) Cell-fate determination by ubiquitin-dependent regulation of translation. *Nature* **525:** 523-527
Woodruff JB, Ferreira Gomes B, Widlund PO, Mahamid J, Honigmann A, Hyman AA (2017) The Centrosome Is a Selective Condensate that Nucleates Microtubules by Concentrating Tubulin. *Cell* **169:** 1066-1077 e1010
Yamazaki H, Takagi M, Kosako H, Hirano T, Yoshimura SH (2022) Cell cycle-specific phase separation regulated by protein charge blockiness. *Nat Cell Biol* **24:** 625-632
Yao RW, Xu G, Wang Y, Shan L, Luan PF, Wang Y, Wu M, Yang LZ, Xing YH, Yang L, Chen LL (2019) Nascent Pre-rRNA Sorting via Phase Separation Drives the Assembly of Dense Fibrillar Components in the Human Nucleolus. *Mol Cell* **76:** 767-783 e711